Vol. 284: 77–96, 2004 | MARINE ECOLOGY PROGRESS SERIES
Mar Ecol Prog Ser | Published December 21

Real-time observation of taxa-specific plankton distributions: an optical sampling method

Cabell S. Davis[1,*], Qiao Hu[2], Scott M. Gallager[1], Xiaoou Tang[3], Carin J. Ashjian[1]

[1]Department of Biology, and [2]Department of Applied Ocean Physics and Engineering, Woods Hole Oceanographic Institution, Woods Hole, Massachusetts 02543-1541, USA

[3]Department of Information Engineering, The Chinese University of Hong Kong, Shatin, N.T., Hong Kong, SAR

ABSTRACT: A fundamental problem in limnology and oceanography is the inability to measure the taxonomic composition of plankton quickly over a broad range of scales. Traditional sampling with bottles and nets provides critical data at the species-level, but has limited spatio-temporal coverage and can destroy ubiquitous delicate forms. To augment traditional sampling, recent advances in bioacoustics and non-imaging optics provide real-time high-resolution data on biomass abundance and size composition. New optical imaging approaches provide coarse taxonomic composition but require manual image identification, preventing real-time observation. Here, we describe a method of optical sampling and analysis, using the Video Plankton Recorder, to automatically identify plankton to major taxa (and to species in some cases) and observe their distributions at sea in real time. We present a detailed assessment of classifier accuracy, including a comparison of machine- and hand-classification of images. The automated classification method was found to be sufficiently accurate for estimating abundance patterns of dominant taxa but not for less abundant taxa. The range in overall accuracy was 60 to 70% for 7 taxa and 79 to 82% for 2 taxa, with accuracies for individual taxa ranging between 45 and 91%. Classification error was small relative to natural variability in abundance of dominant taxa. For a given taxon, the error in the abundance estimate was low in regions of high relative abundance. A manual correction step can be used in areas of low relative abundance to obtain accurate abundance estimates. Example data from 2 cruises are presented to illustrate the utility of real-time taxa-specific data collection. These data represent the first real-time automatic identification and mapping of plankton taxa at sea. This methodology represents an intermediate step towards the ultimate goal of real-time identification of plankton to the level of species and life stage. At present, optical imaging methods cannot replace net and bottle surveys, but can be used to obtain coarse taxonomic composition of plankton (including fragile forms) with an identification accuracy that is high enough to produce quantitative high-resolution maps of abundant taxa in real time.

KEY WORDS: Plankton · Video · Sampling · Pattern recognition · Image analysis · Real time

INTRODUCTION

It is well known that plankton distributions are patchy in nature and that high-resolution sampling is required to resolve the patchiness (Fasham 1978, Haury et al. 1978, Omori & Ikeda 1984, Mackas et al. 1985). The large effort involved in sample collection and analysis, however, sets limits on sampling intensity. Plankton surveys can generate hundreds or thousands of samples, requiring months or years of analysis (Sherman 1980, Warner & Hays 1994, Ohman & Smith 1995) and still may not have sufficient sample density for quantification of patchiness (Huntley et al. 1995). Thus, while traditional sampling provides essential data on species and life stages that are presently unattainable by other methods, newer automated methods

*Email: cdavis@whoi.edu

are being developed to augment this sampling with rapid high-resolution data acquisition.

Automated high-resolution sampling methods, including fluorometry, and acoustical and optical particle counters, have been developed to quantify abundance patterns of total plankton (Denman & Herman 1978, Holliday et al. 1989, Herman 1992, Wiebe et al. 1996), and these methods have led to insights into factors controlling patchiness (Platt & Denman 1978) and more generally pelagic ecosystem size structure (Silvert & Platt 1980, Sprules & Munawar 1986). These sampling methods do not as yet distinguish between taxonomic groups of plankton but do provide critical data on bulk plankton and particulate properties.

A greater understanding of pelagic ecosystems requires high-resolution data on the abundance of planktonic taxa in relation to their associated environmental variables over a broad range of scales (Marine Zooplankton Colloquium 1989). The focus in plankton ecology on population and predator–prey dynamics requires taxa-specific information (Davis 1984, 1987, Rothschild 1988, GLOBEC 1991). The dynamical nature of both the biological and physical components of pelagic environments necessitates rapid high-resolution sampling, while the large size of these ecosystems in relation to the small size of the individual organisms requires sampling a wide range of scales.

Advances in optical imaging have led to the development of sampling systems such as the Video Plankton Recorder (VPR) that are being used to determine abundance and behavioral patterns of plankton (Davis et al. 1992a,b, Schulze et al. 1992, Gallager et al. 2004). These systems have several advantages, including the ability to identify planktonic taxa, measure distributions nearly continuously over a broad range of scales, and sample delicate plankton and particulate matter. A current limitation of optical imaging systems is that they do not yet have the resolving power to identify plankton to the level of species and life stage. Nonetheless, optical imaging now can provide important information on coarse taxonomic composition and abundance of distinctive taxa. Importantly, these new systems acquire images in an electronic format that is suitable for automatic processing. Data acquired from these systems to date have been obtained largely by manual analysis of the video, a tedious and time-consuming process (Benfield et al. 1996, Davis et al. 1996, Gallager et al. 1996, 2004, Norrbin et al. 1996, Ashjian et al. 2001).

Although such manual analysis is labor-intensive, these VPR studies have yielded high-resolution data on distributional patterns of plankton taxa and marine snow in relation to environmental variables. Abundance estimates from spatially averaged VPR data have been shown to agree closely with abundance estimates from standard net sampling systems (e.g. MOCNESS) for dominant non-fragile zooplankton taxa (e.g. copepods) (Benfield et al. 1996, Gallager & Davis 2003). By contrast, quantification of delicate forms such as colonial radiolaria (Dennett et al. 2002), larvaceans (Benfield et al. 1996), marine snow (Ashjian et al. 2001) and algal colonies (Sieracki et al. 1998, Villareal et al. 1999) has revealed that the non-destructive nature of video sampling provides more accurate abundance estimates, which can be up to 2 orders of magnitude greater than estimates from traditional net and bottle samplers. Video samplers, however, have a much smaller sampling volume than do plankton nets, and can undersample rare organisms (e.g. <50 ind. m^{-3} for the high-magnification VPR camera, Benfield et al. 1996).

Current plankton imaging systems have taken a long time to develop. Sir Alistair Hardy suggested as early as 1956 that underwater television is an important new tool 'which promises much for the future' (Hardy 1956). Video imaging of plankton has only recently become a reality, and real-time automatic processing of the video from image to taxa-specific densities has not yet been achieved due to the time-lag involved in development and integration of image processing hardware and software. As an intermediate step, a semi-automated method for quantifying plankton distributions using the VPR was developed, requiring manual identification of plankton images extracted from the video by an image processing system (Davis et al. 1996). More recent algorithms have been developed for automatic identification of planktonic taxa from video images (Tang et al. 1998), but these algorithms have not been used for their ultimate purpose: real-time identification of plankton in the field. The accuracy level of these classifiers was found to be promising, but was based on a small set of images and accuracy was not thoroughly examined.

In the current paper, we describe in detail a method for acquiring real-time data on coarse taxonomic composition and abundance of dominant major groups of plankton. We present example data from 2 cruises that demonstrate, for the first time, real-time automatic quantification of taxa-specific plankton distributions. Finally, we analyze in detail the accuracy of the plankton classification method.

The paper includes an initial overview of the VPR system and a description of the real-time automatic identification and classification accuracy assessment. Example data then are presented from cruises to Georges Bank on the R/V 'Endeavor' in June 1997 (EN302) and June 1999 (EN323). Data from the first cruise are used in a detailed analysis of the accuracy of automatic versus manual classification of the images.

MATERIALS AND METHODS

VPR system overview. The VPR system includes an underwater unit with video and other sensors, and a deck unit for data logging, processing and display (Fig. 1). For the studies reported here, the VPR underwater unit consisted of 2 analog video cameras (high and low magnification) synchronized at 60 Hz to a xenon strobe, environmental and flight control sensors sampling at 3 to 6 Hz (pressure, temperature, salinity, fluorescence, beam attenuation, downwelling light, pitch, roll, velocity and altitude), and a data telemetry system. The cameras, strobe and sensors were mounted on a frame attached to the bottom of a 1.22 m V-fin depressor. The underwater unit was towed at 4 m s^{-1} using a 1.73 cm (0.68 in) diameter triple-armor electro-optical cable. A fiber-optic transmitter sent video and sensor data to a receiver mounted in the winch drum on the ship where it subsequently passed through electrical slip rings and deck cable to the deck unit in the ship's lab.

The deck unit (Fig. 1) consisted of a video recording/display system, an environmental/navigational data logging system, an image processing system and a data display system. Video was time-stamped at field rates (60 fields s^{-1}, fps) and recorded on SVHS recorders. The video time code was synchronized with time from the P-code Global Positioning System data string. Latitude and longitude were logged together with video time code and the VPR environmental data at 3 Hz on a PC and a Silicon Graphics Inc (SGI) workstation.

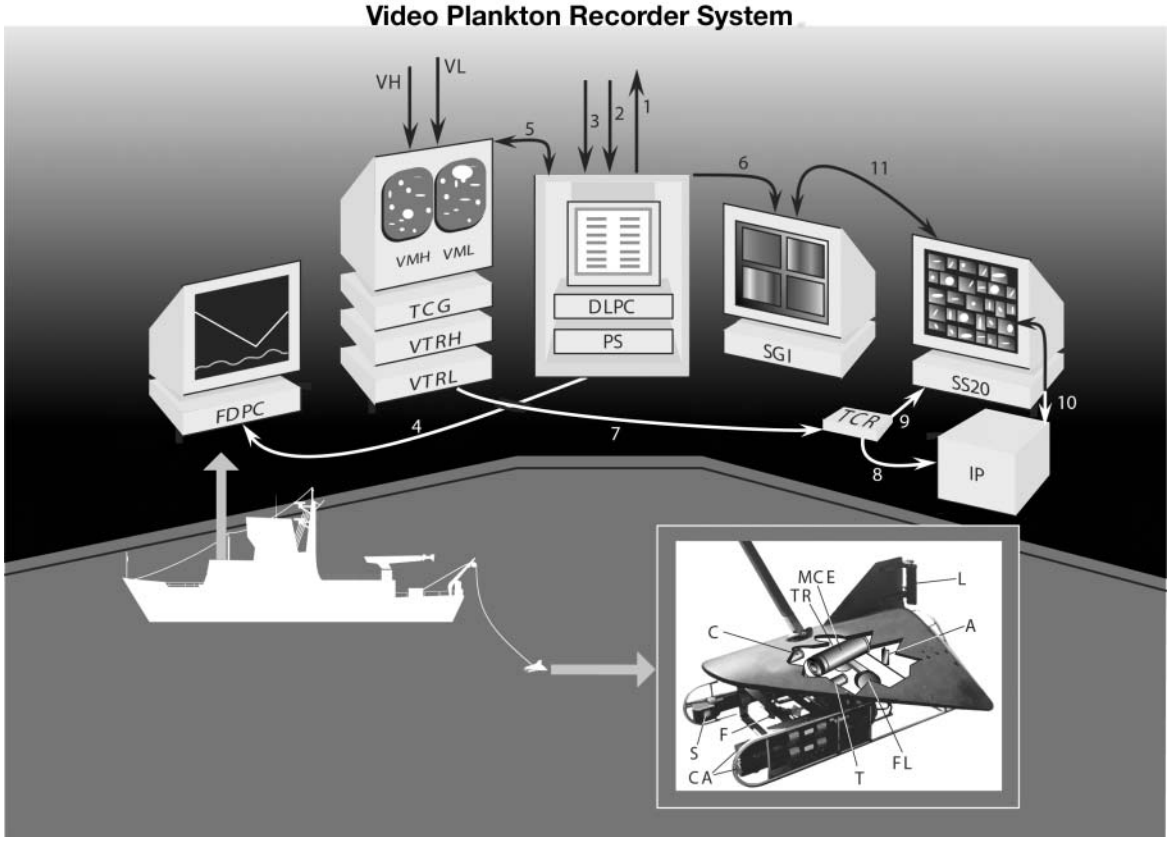

Fig. 1. Video Plankton Recorder system showing underwater and shipboard components. The VPR is towyoed at ship speeds up to 4 m s^{-1}, while video is processed on board to extract in-focus images, identify them to major taxa and display their distributions. Abbreviations are: Shipboard Unit—FDPC = flight display PC, VH = Video input High magnification, VL = Video input Low magnification, VMH = Video Monitor High magnification, VML = Video Monitor Low magnification, TCG = Time Code Generator, VTRH = Video Tape Recorder High magnification, VTRL = Video Tape Recorder Low magnification, DLPC = Data Logging PC, PS = Power Supply, SGI = Silicon Graphics Inc. workstation, TCR = Time Code Reader, SS20 = Sparcstation 20, IP = Imaging Technologies Image Processor, 1 = power out to underwater unit, 2 = environmental sensor data from underwater unit, 3 = navigational data from ship (latitude, longitude, bottom depth), 4 = data out to flight display computer, 5 = serial time code from TCG to DLPC, 6 = environmental and navigation data to SGI, 7 = video to time code reader, 8 = video from TCR to image processor, 9 = serial time code to SS20, 10 = data transfer between SS20 and IP, 11 = data transfer between SGI and SS20. Underwater unit—C = conductivity sensor, TR = Transmissometer, MCE = Main Control Electronics, L = Light sensor, A = Altimeter, FL = Fluorometer, T = Temperature sensor, CA = Cameras (high and low magnification), F = Flowmeter, S = Strobe

Image processing. Image processing consisted of in-focus object detection, object feature extraction and object feature classification. The methods used for each step are as follows.

Detection of in-focus objects: Video (with time code) from a selected camera was sent to the focus detection system, which included an image processor (Imaging Technology, Models 151 and 150-40) interfaced to a computer (Sun Sparcstation or Pentium PC). Video was digitized at field rates (60 Hz), in-focus objects were detected using an edge detection method, and sub-images comprising the region of interest (ROI) were saved to the computer disk as tagged image format files using the video time code as the filename. In this way each ROI was time-stamped for subsequent spatial mapping[1].

The 'in-focus' volume is contained within the strobe beam such that video images include illuminated but out-of-focus portions of the light beam, thus requiring a step to select only in-focus objects. Focus detection was used to capture subimages of only those objects contained within the depth of field (DOF). The DOF was determined in a laboratory calibration by moving a tethered copepod measured distances towards and away from the camera, while using the focus detection system to objectively determine whether the animal was in or out of focus. The DOF was determined in the center of the field of view (both cruises) and additionally in each of the 4 corners (for EN323) to account for any uneven illumination across the field. DOF measurements were used together with measurements of field width and height to objectively quantify the imaged volume (see Davis et al. 1992a). Total volume (ml) is defined by: $V = 1/6 \times W \times H \times (2 \times D_C + D_1 + D_2 + D_3 + D_4)$, where W is field width (cm), H is field height (cm) and D is the depth of field (cm) at the center and 4 corners of the field of view. For the 2 cruises discussed here, calibrated image volumes were 0.50 ml for the high-magnification camera on EN302 and 7.16 ml for the low-magnification camera on EN323.

In-focus object detection involves brightness correction, segmentation, connectivity, labeling, size thresholding, edge detection, coalescing and ROI generation. Incoming images are dynamically adjusted to correct for temporal changes in mean brightness by translating the pixel brightness values so that the mean is 125. Translation is used rather than scaling (normalization) to avoid changing brightness gradients within the image. Brightness correction is followed by segmentation, which involves binarization of the grey-scale image such that pixels above a certain brightness threshold are given a value of unity and zero otherwise. After segmentation, a connectivity algorithm determines which non-zero pixels are connected to each other in a 'blob'[2]. The distinct blobs then are 'labeled' or numbered from 1 to N, where N is the number of blobs present. Since many small blobs (e.g. single pixel) are created this way, a size threshold is imposed so that only blobs above a minimum number of pixels are processed. A rectangular bounding box is then placed around each blob and the brightness gradient at each pixel in the box is determined using a Sobel operation (Pingle 1969, Pratt 1976). If the average brightness gradient of the blob pixels is above a threshold value, the blob is considered in focus. Since planktonic organisms usually are partially transparent or translucent, their images when binarized often comprise several smaller blobs. A coalesce algorithm is applied to group in-focus blobs that are in close proximity to each other. A ROI containing each group of coalesced blobs (including a specified proportion of marginal space around the group) is written to disk.

Object feature extraction: Object feature extraction algorithms operate on the ROI files and generate a feature file for each ROI. Automatic brightness correction, segmentation and connectivity are performed again on each ROI file to determine the position of blob pixels in the ROI. The smallest rectangular bounding box that can fit around the blob at any angle is determined. Morphological measurements computed for each ROI include P (perimeter = number of edge pixels in blob), A (area = total number of pixels in blob), L_1 (longest dimension of bounding box), L_2 (shortest dimension of bounding box), W_{center}, $W_{left\,1/4}$, $W_{right\,1/4}$ (widths of the blob at $\frac{1}{2}L_1$, $\frac{1}{4}L_1$, and $\frac{3}{4}L_1$), u_{20}, u_{02}, u_{11} [central moments = $\sum(x-\bar{x})^2$, $\sum(y-\bar{y})^2$, $\sum(x-\bar{x})(y-\bar{y})$, where x and y are pixel coordinates of perimeter], E_1, E_2 (rotation invariant principal moments = $\sum y'y'$, $\sum x'x'$, where x' and y' are x and y rotated through θ), θ (angle of major principal moment axis to horizontal).

Features included shape factor $\left(P^2/(4 \times \pi \times A)\right)$, the 7 invariant moments (Hu 1962, Gonzalez & Wintz 1987), Fourier descriptors (Zahn & Roskies 1972), granulometric curves (Vincent 1993) and the ratios E_1/E_2, L_1/L_2, W_{center}/L_2, $W_{left\,1/4}/L_2$, $W_{right\,1/4}/L_2$. These features are combined into a single feature vector totaling 237 elements. Principal component analysis is then used to eliminate linear-dependence among elements of the feature vector (for details, see Tang et al. 1998). The

[1]This image processing system recently has been converted to a software-based system where a simple frame-grabber card is used to digitize the video and the focus detection is done in software running on a Pentium processor

[2]The term 'blob', derived from 'Binary Large OBject' or sometimes 'Binary Little OBject', is used in image processing to refer to a distinct group of 1 or more white (or black) pixels in a binary image that are touching one another but are not touching other such groups

first 20 to 30 components account for nearly all the variance in the training sample feature space. These EOFs are applied to the feature vectors of the non-training ROIs to obtain transformed feature vectors of 20 to 30 linearly independent elements.

Object classification: For classification, a neural network classifier was first trained by manually sorting a set of representative ROIs into different taxonomic groups, extracting and transforming their feature vectors, and using the Learning Vector Quantization (LVQ) method (Kohonen et al. 1988) to fit neurons to these transformed feature vectors. The resulting classifier was then used to automatically sort the remaining ROIs. Since the neural network classification involves only a series of multiplications, it is very fast. Classifier accuracy was determined for each of the VPR tows presented below.

Output from the classification system generated a list of time codes for each taxon. The classifier operated on a second computer (SGI or PC) and the output was saved to disk.

Data display. Distributional data for the observed taxa and environmental variables were displayed at sea in real time. The data display system, also operating on the second computer, read the output of the neural network classifier from the disk files, binned the time codes into 4 or 10 s bins, and time-matched these data with the navigational and environmental data, yielding the latitude, longitude and depth of each bin. The abundance (number of ind. l^{-1}) of a given taxon was determined from the number observed in each time bin divided by the volume imaged (e.g. 10 s × 60 fps × 0.5 ml = 0.30 l for the high-magnification camera in EN302). The ship speed was fast enough that the fields were non-overlapping. The abundance then was plotted in Matlab (Mathworks) as a scatter plot of depth versus along-transect distance, with dot color corresponding to abundance level. Using the same dot-color scheme, abundance also could be plotted as depth versus elapsed time or as a 3D scatter plot of depth versus latitude and longitude. In other windows of the computer screen, environmental data were displayed using the same color dot-plot method. This technique allows direct side-by-side comparison of the distribution of a planktonic taxon with the associated environmental variables in real time as the tow is progressing. We also have objectively mapped (e.g. kriged) the data and displayed it in volume-rendered plots, but for the purposes of this paper we limit display of example real-time data to the dot-plots to avoid confusion from interpolation/smoothing.

Classification error analysis. A detailed analysis of the automatic classification error rate was performed in the laboratory after the cruises. Particular emphasis was placed on VPR 7, a 24 h tow in the Great South Channel, in which we had obtained the first real-time taxa-specific plankton data. The classification error rate or simply the error rate, P_e, is the ultimate measure of the performance of a classifier. There is no single best way to measure the error rate. In practice, the error rate is measured by building a confusion matrix for the classifier. The confusion matrix is an $N \times N$ matrix, where N is the number of taxa or classes in the classifier. Each element of the matrix is the true number of Class j that is classified as Class i. The confusion matrix is a way to measure the conditional probability that a sample belonging to Class j is classified as Class i. The confusion matrices were built using 3 different methods, including resubstitution, holdout and cross-validation (see below, this subsection).

A series of tests was conducted to assess the effect of various factors on classification accuracy. These tests included assessment of the at-sea classifiers used during the cruises as well as subsequent classifiers built in the laboratory after the cruise. Factors examined included the method of quantifying classifier accuracy, the source of the training ROIs (same tow or different tows), the number of training ROIs (both total number and distribution among taxa), random versus ad hoc selection of training ROIs, the number of neurons used to build the classifier, neuron dimension (feature length) and the use of an 'other' category versus neuron-distance rejection methods. We also examined classifier variability resulting from randomization of initial neuron position and presentation order of the training samples to the LVQ algorithm.

The accuracy of the original classifiers built at sea during the cruise was determined using the resubstitution and cross-validation methods (Cover 1969, Fukunaga & Hummels 1989, Jain et al. 2000). The resubstitution method simply classifies the training ROIs that were used to build the classifier, so this method obviously yields accuracy estimates that are biased towards the high end when compared to the true accuracy of classifying the non-training ROIs. The resulting confusion matrix then is the number of classified ROIs versus the number of hand-sorted training ROIs. The cross-validation method (also termed the 'leave-one-out' method; Fukunaga & Hummels 1989) provides a better estimate of the true accuracy. This method also uses only the set of training ROIs to assess the classifier accuracy, but instead of using all the training ROIs at once to build 1 classifier, multiple classifiers are built. An initial classifier is built using all the ROIs in the training set except 1. This classifier is then used to classify the left-out ROI. This process is then repeated for every ROI in the training set and the results tallied in the cells of the confusion matrix.

After the EN302 cruise, during post-processing, a new training set was made by sorting ROIs from several different tows in an ad hoc fashion until 200 to 250

training ROIs had been sorted for each taxon. During this sorting process, additional taxa were found to be abundant, and thus were added to the training set. A classifier was built using these new training ROIs and used to reclassify all the ROIs in VPR tow 7. Confusion matrices were developed to determine the accuracy of this classifier compared with the real-time classifier.

Finally, to determine the true classifier accuracy, all 20 399 ROIs from VPR Tow 7 (EN302) were manually sorted and subsets containing 200 ROIs per taxon were randomly selected for the training set. Confusion matrices then were built and compared for resubstitution, cross-validation and a third method, called the hold-out method (Fukunaga & Hummels 1989, Jain et al. 2000). In the latter method, the classifier built using the 200 randomly selected training ROIs per taxon was used to classify the remaining, non-training ROIs, so that a confusion matrix could be developed by directly comparing the automatically classified ROIs with the manually sorted ones. In this case, since none of the manually sorted ROIs was used to build the classifier, it provides the truest estimate of classifier accuracy (assuming the human classification was perfect, but see Culverhouse et al. 2003).

In addition to assessing methods for quantifying classifier accuracy, the effects of other factors affecting classifier accuracy were examined. These factors included feature length, neuron number and relative abundance of taxa. Classifiers were built using 6, 10 and 20 neurons per taxon for a total number of 42, 70 and 140, respectively. The initial post-cruise training set of 200 to 250 ROIs per taxon (from different tows) was used to build these classifiers. Additional tests of the effect of neuron number were performed for the other tows.

The effect of using the same number of training ROIs for all taxa (e.g. 200) versus having the number of training ROIs proportional to mean abundance of each taxon was examined using the post-cruise data set (VPR 7) in which all ROIs had been hand-sorted. The effect of using 200 training ROIs per taxon but weighting the resulting neurons by the proportion of the taxa in the tow also was examined. The latter weighting method was applied using the mean proportion for the whole tow as well as weightings based on the running average of the taxonomic proportions throughout the tow.

Beyond classifier accuracy per se, we needed to develop a method to correct for the statistical bias we found to be inherent in quantifying relatively rare taxa, i.e. false-negative identification of abundant taxa causes overestimation of rare taxa. We presented a statistical method to correct for this bias elsewhere (Solow et al. 2001) and the effects on our data are given below. The method assumes an unbiased classifier (one built from representative training samples) and uses the error rate determined by cross-validation to correct relative abundance errors.

Field sampling. We have used the automated VPR system routinely to quantify distributional patterns of dominant planktonic taxa at sea in real time. Here, we present examples of distributional data of planktonic taxa during cruises to Georges Bank in June 1997 and June 1999. These cruises were part of the US Global Ocean Ecosystem Dynamics (GLOBEC) Georges Bank Study of the biological/physical processes controlling copepod and larval fish abundance in this important fishing ground. Results are presented for phytoplankton and zooplankton taxa from study sites in the Great South Channel (GSC) in 1997 and from a frontal mapping study along the edge of the well-mixed area on the crest of Georges Bank (GB) in 1999 (Fig. 2). During the GSC study, sampling was conducted over 24 h back and forth along a 40 km east/west transect from the crest of the bank to the center of the channel to measure plankton populations as they moved through the channel (in tidal time) and recirculated around the bank. This transect was sampled 12 times during the 24 h period. During the George Bank frontal study in 1999, the VPR was towyoed (hauled up and down using the winch) along a zigzag grid centered on the tidal mixing front. In these studies, the VPR was continuously towyoed from near surface to within 5 to 10 m of the bottom while the ship steamed at 4 m s^{-1}.

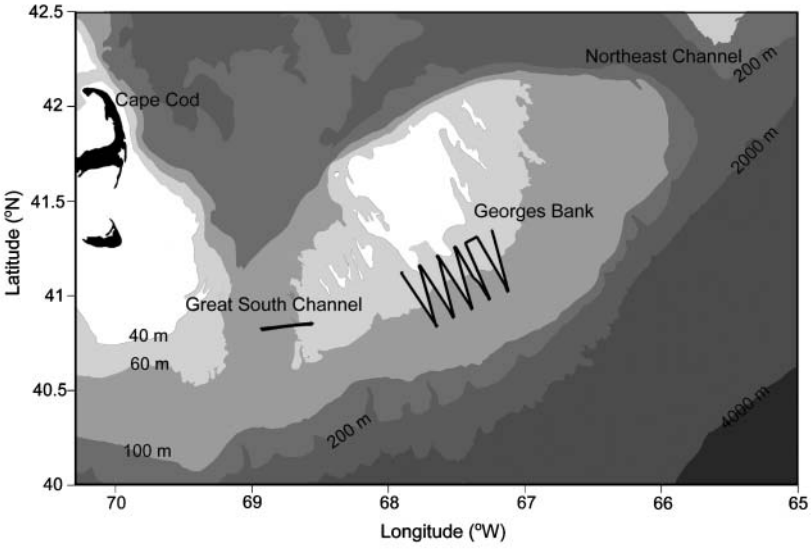

Fig. 2. Map of study area showing locations of VPR data collection at the 2 study sites: Great South Channel (GSC) and Georges Bank (GB)

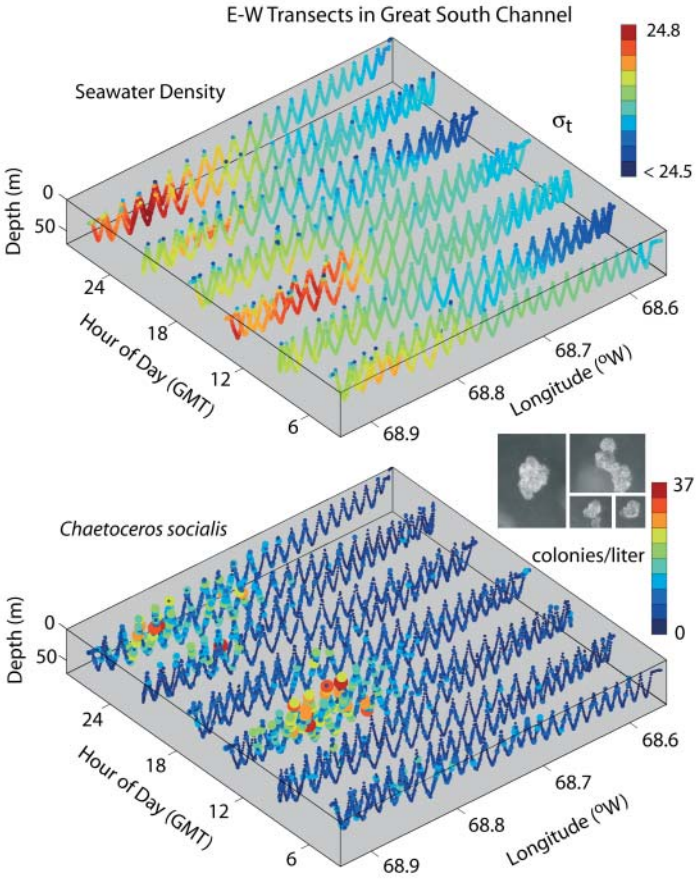

Fig. 3. Data from GSC study, June 17 (03:11 h GMT) to 18 (03:53 h), 1997. 3D dot plots of seawater density and *Chaetoceros socialis* abundance show the time–space evolution of the tow. Dots correspond to 3 Hz data decimated to 4 s. Dot size for *C. socialis* is directly proportional to abundance. Also shown are VPR images of *C. socialis* colonies

RESULTS AND DISCUSSION

Real-time observation of distributional patterns

In this section, example data are presented to demonstrate the use of optical sampling as a method for acquiring taxa-specific abundance information at sea in real time[3].

Great South Channel

During this study, a region of higher-density water (lower temperature and higher salinity) was observed to enter the western end of the transect during the latter part of each 12 h tidal cycle (Fig. 3). This water contained high concentrations of the colonial diatom *Chaetoceros socialis* (Fig. 3), a dominant phytoplankton species in coastal systems of the North Atlantic. This fragile species has a distinctive appearance on the video images, and VPR observations have been corroborated at sea using bottle collections and microscopic analysis (see Sieracki et al. 1998)[4]. Previously during the cruise, a grid survey of the region just south of this transect line had revealed a large patch of *C. socialis*. The GSC study indicated that the NW edge of this patch moved back and forth through the transect with the tidal flow (Fig. 3). The close association of the *C. socialis* patch with seawater density and its movement with the tidal flow indicated that physical factors were controlling the distribution of *C. socialis* over these short time and space scales. The patch of *C. socialis* had become more diffuse by the second tidal cycle (Fig. 3). The sudden appearance of high *C. socialis* abundance toward the end of the 5th transect leg was a surprise, since such high concentrations had not been observed during the first 4 legs. This high concentration clearly was associated with high-density water advected northward. The high abundance was obvious in real-time as evidenced by the large numbers of *C. socialis* colonies appearing in the video and by the quantitative real time color dot plots (Fig. 3). The ship departed from this patch during the end of the 5th leg but re-entered it shortly after turning eastward again on the 6th leg (Fig. 3). The patch had disappeared by the 7th leg, leading to the conclusion that it was tidally transported, and to the (correct) prediction by observers on board the ship that the patch would be seen again during the next tidal phase (12 h) (Fig. 3).

Georges Bank

The frontal mapping study was designed to quantify the 3D distributional patterns of *Calanus* and other plankton in the tidal mixing front of GB (Fig. 4). These data were incorporated into a real-time data assimilative biological/physical model of cross-frontal exchange running on board the ship (McGillicuddy & Kosnyrev 1999, Lynch et al. 2001). The data also were used to determine locations of high abundance of *Calanus* for a tracer release/patch study (rhodamine dye injection and tracking; Ledwell 1999). The real-time distributional data for *Calanus* and planktonic hydroids shows the inverse spatial relationship between these 2 taxa (Fig. 4). *Calanus* were more abun-

[3]Hypotheses and objectives for these GLOBEC cruises are given in Beardsley et al. (1992)

[4]*Chaetoceros socialis* colonies are very fragile and are not sampled quantitatively using conventional methods. We found that the colonies are easily destroyed when sampled through the spigot of a Niskin bottle but could be collected with less damage by siphoning them gently out of the top of the bottle (S.M.G. pers. obs.)

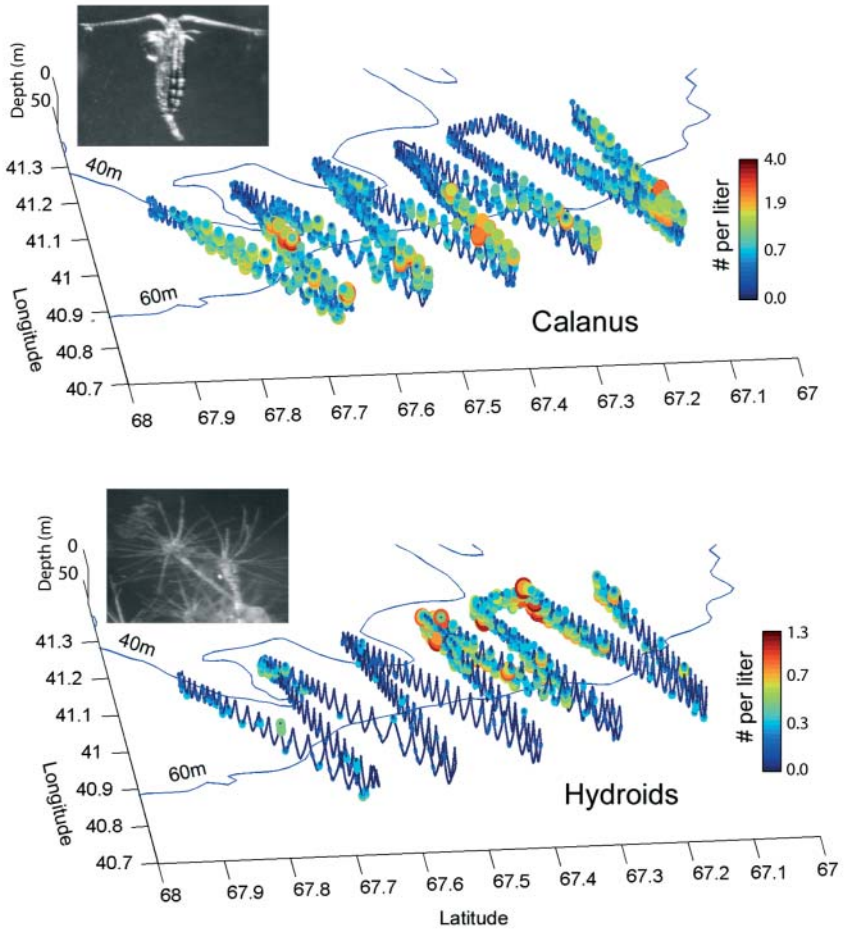

Fig. 4. Data from the frontal mapping study on GB, May 8 (06:40 h GMT) to 9 (08:20 h), 1999. Upper and lower panels show the distributions of *Calanus* and hydroids, respectively. Dot size and color are directly proportional to abundance. Data are from the low-magnification camera. VPR images of *Calanus* and hydroid polyps (from the high-magnification camera) also are shown

dant on the deeper south side of the front, while the predatory hydroids were more abundant on the shallower north side (Fig. 4). This survey ran from east to west and took 24 h to complete, during which time the semi-diurnal tidal excursions (~6 km) caused time–space aliasing in the data. Thus, the lower abundance of hydroids in the NW half of the survey was due, at least in part, to northward tidal flow reducing the amount of well-mixed water in this portion of the grid. When these data were assimilated into the model as time-space points, the aliasing was removed and corrected distributional patterns were computed (McGillicuddy & Kosnyrev 1999, Lynch et al. 2001).

The GSC and GB studies demonstrate that optical imaging technology can be used effectively to acquire taxa-specific plankton abundance data at sea in real time. Such a capability is useful for on-board data assimilative modeling studies and for interactive at-sea sampling strategies.

Identification accuracy

Manually identified images

The accuracy of the automatic classifier was examined for each VPR deployment. In order to directly compare the automatic classification results with human-classified results, all 20 399 ROIs collected during the 24 h GSC tow (June 1997; Fig. 3) were both hand-sorted and automatically classified. These VPR images initially were sorted into 17 taxa and these taxa were subsequently grouped for the analyses (Table 1). The taxa were grouped together because the rarer taxa had too few individuals and because the present classification method is not accurate enough to distinguish between genera.

Example images

Each of the resulting taxonomic categories was distinct and could be readily identified by a human expert (Fig. 5). The ROIs displayed in Fig. 5A include individuals from each taxon randomly selected from the GSC ROI set. As described in the 'Materials and methods' section, the features extracted from these images for automatic classification were scale- and rotation-invariant. Hydroid medusae were the largest of the taxa and had distinctive bell and tentacles (Fig. 5A). Like the other taxa, they were variously oriented in 3D and thus presented a range of 2D projections in the video images. In addition, owing to their relatively large size (4 to 5 mm bell diameter), usually only a portion of their bodies were present in the images (Fig. 5A). The next largest categories were *Chaetoceros* chains and marine snow (Fig. 5A). *Chaetoceros* chains were typically 1 to 5 mm long and often curved with distinctive spines that scattered light well. Marine snow also exhibited a large range of sizes (1 to 5 mm) and had distinctive darker regions of optically dense matter resulting from their non-living detrital nature (Fig. 5A). The remaining taxa were smaller and included copepods, *C. socialis* colonies, rod-shaped diatom chains and a category for all others (Table 1). Copepods were distinguished visually by a combination of their prosome, urosome and/or antennules, while *C. socialis* colonies were easily recognized by their shape and texture (Fig. 5A). Rod-shaped diatom

Table 1. List of taxa sorted from VPR images collected in the Georges Bank/Gulf of Maine Region during May/June 1997 and 1999

At-sea	Post-cruise EN302 VPR 7	
EN302 VPR 7	**All sorted taxa**	**7-taxa training set**
1 Copepod	*Calanus*	**1** Copepod
2 Rod-shaped diatom chains	*Centropages*	
3 *Chaetoceros socialis* colonies	*Oithona* with eggs	
4 Hydroid medusae	*Pseudocalanus* with eggs	
5 Blank	*Oithona*	
	Unidentified copepods	
EN323 VPR 3	Rod-shaped diatom chains	**2** Rod-shaped diatom chains
1 *Calanus*	*Chaetoceros* chains	**3** *Chaetoceros* chains
2 Other copepods	*Chaetoceros socialis*	**4** *Chaetoceros socialis*
3 Hydroid colonies	Hydroid medusae	**5** Hydroid medusae
4 Unknown ovals	Marine snow	**6** Marine snow
5 Pseudocalanus with eggs	Coil-shaped diatom chains	**7** Other
6 Pteropods	Ctenophores	
7 Unfocused	Chaetognaths	
	Polychaetes	
	Copepod nauplii	
	Other	

Table 2. Confusion matrices for EN302, VPR Tow 7, based on real-time (at-sea) classifier and computed using (A) resubstitution and (B) cross-validation methods. Column and row headings are coded as: 1 = copepod, 2 = rod-shaped diatom chains, 3 = *Chaetoceros socialis* colonies, 4 = hydroid medusae, 5 = blank, TC = Total Computer count, TH = Total Human count, A = Accuracy (% true positive, also known as probability of detection), C/H = Computer/Human total count. True counts (i.e. human counts) for a given taxa are given in the columns, while counts by automatic identification (= computer) are given in the rows. For example, in Table 2a, 364 copepods were identified correctly by the computer, whereas 5 copepods were misclassified by the computer as being rod-shaped diatoms. Likewise 934 *Chaetoceros socialis* were correctly identified by the computer whereas 6 *C. socialis* were incorrectly identified by the computer as being copepods. Thus, correct identifications by the computer are given along the main diagonal, while the off-diagonal entries are the incorrect identifications by the computer

	1	2	3	4	5	TC
(A) Resubstitution						
1	**364**	1	6	4	1	376
2	5	**88**	4	0	12	109
3	21	3	**934**	7	26	991
4	7	0	3	**66**	0	76
5	4	2	19	2	**341**	368
TH	**401**	**94**	**966**	**79**	**380**	**1920**
A	91	94	97	84	90	93
C/H	0.94	1.16	1.03	0.96	0.97	1
(B) Cross-validation						
1	**328**	8	17	16	2	371
2	13	**69**	2	0	12	96
3	51	9	**883**	23	59	1025
4	6	1	12	**36**	2	57
5	3	7	52	4	**305**	371
TH	**401**	**94**	**966**	**79**	**380**	**1920**
A	82	73	91	46	80	84
C/H	0.93	1.02	1.06	0.72	0.98	1

chains also were readily identifiable (Fig. 5A). Objects that were either unrecognizable and/or uncommon were grouped into an 'Other' category (Fig. 5A).

For the GB frontal study, images from the low-magnification camera were used. Dominant taxa used in training were *Calanus*, *Pseudocalanus* with eggs, other copepods, pteropods, hydroid colonies and unknown oval-shaped objects (possibly meroplanktonic larval forms) (Table 1, Fig. 5B). Although the images were much smaller and contained fewer pixels, the taxa were easily distinguished at this magnification (Fig. 5B). Since the focus detection algorithm was not perfect, a certain portion of the ROIs were out of focus. To automatically separate these ROIs, a 7th, 'unfocused', category was added.

Accuracy of at-sea classifiers

The classifier used at sea during the GSC study was found to have an overall accuracy for true positives of 93 and 84% for resubstitution and cross-validation methods, respectively (Table 2). As discussed in the 'Materials and methods' section, cross-validation is a truer estimate of accuracy for classification of non-training ROIs[5].

The first real-time, at-sea, automatic classification of plankton was successfully performed during this GSC study. Highest identification accuracy was obtained for *Chaetoceros socialis* colonies (91%), so that the real-time plot of this species (Fig. 3) can be

[5]As shown below, however, the cross-validation method is biased when training samples are not representative

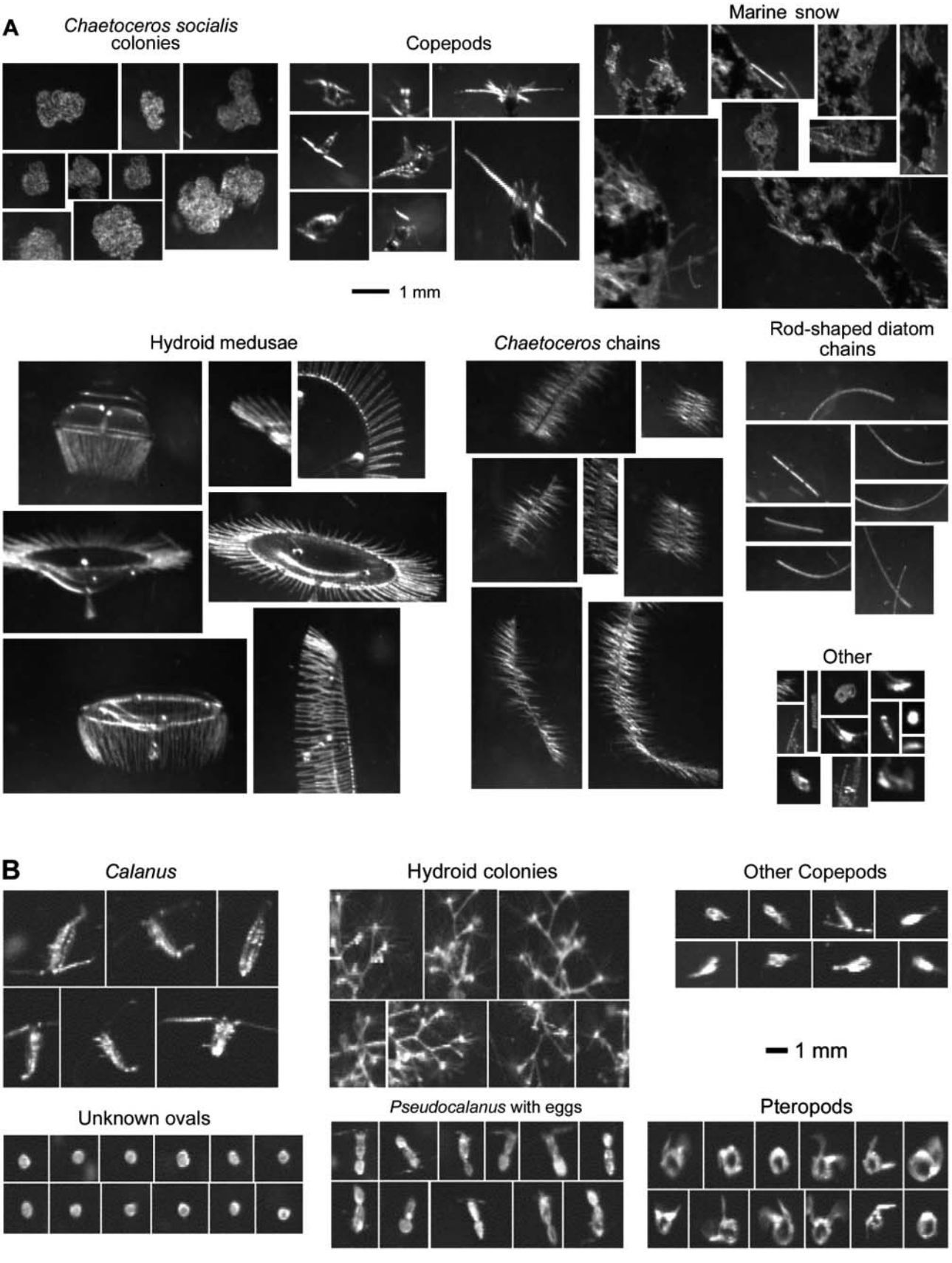

Fig. 5. Example VPR images from the 2 study sites. (A) Images from the Great South Channel study (high-magnification camera). Randomly selected images of each taxon are shown. (B) Images from the Georges Bank frontal study (low-magnification camera)

Table 3. Confusion matrix for EN323, VPR-3, based on at-sea classifier and computed using: (A) resubstitution and (B) cross-validation methods. Column and row headings are: 1 = *Calanus*, 2 = Other copepods, 3 = hydroid colonies, 4 = unidentified ovals, 5 = *Pseudocalanus* with eggs, 6 = pteropods, 7 = unfocused, TC = Total Computer, TH = Total Human, A = Accuracy (%), C/H = Computer/Human

	1	2	3	4	5	6	7	TC
(A) Resubstitution								
1	**260**	5	1	0	3	0	1	270
2	4	**194**	1	0	10	4	2	215
3	0	0	**231**	0	0	0	0	231
4	0	2	1	**195**	0	1	11	210
5	7	8	0	0	**192**	3	7	217
6	2	1	1	1	2	**202**	1	210
7	6	3	0	3	5	2	**155**	174
TH	**279**	**213**	**235**	**199**	**212**	**212**	**177**	**1527**
A	93	91	98	97	90	95	87	94
C/H	0.97	1.01	0.98	1.06	1.02	0.99	0.98	1
(B) Cross-validation								
1	**183**	39	11	1	15	18	11	278
2	42	**96**	3	1	46	16	12	216
3	6	3	**215**	0	0	0	5	229
4	1	2	0	**180**	1	3	23	210
5	23	39	1	1	**133**	13	27	237
6	15	13	2	4	7	**155**	7	203
7	9	21	3	12	10	7	**92**	154
TH	**279**	**213**	**235**	**199**	**212**	**212**	**177**	**1527**
A	65	45	91	90	62	73	51	69
C/H	1.00	1.01	0.97	1.06	1.12	0.96	0.87	1

viewed as accurate representations of this species' distributional pattern. This at-sea training set was created quickly, based on 5 categories (it did not include marine snow), and used a limited number (<100) of training ROIs for hydroid medusae and rod-shaped diatom chains (Table 2). Lower accuracy for these latter taxa reflects the reduced number of training ROIs used. Medusae in particular had a low accuracy because the classifier misidentified some of them as *C. socialis* colonies. Portions of each taxon were incorrectly classified by the computer as belonging to the wrong taxa (false negatives), while a similar number of images from the wrong taxa were incorrectly classified as belonging to the correct taxa (false positives). The numbers of true and false positives were similar, so that the computer/human ratio was high for all taxa (Table 2).

For images from the low-magnification camera in the GB study, accuracies were 94 and 69% for resubstitution and cross-validation, respectively (Table 3). In this study, hydroid colonies and unidentified ovals had the highest identification accuracy (90 to 91%), while *Pseudocalanus* with eggs, *Calanus* and pteropods were second highest (62 to 73%). Unidentified copepods and unfocused had the lowest accuracy (45 to 51%); 8% of *Calanus* were misidentified as *Pseudocalanus* with eggs, while 15% were misidentified as other copepods; by contrast, only 5% of hydroid colonies were misidentified as *Calanus*. Thus, the real-time plot of hydroid colonies across the GB tidal front (Fig. 4) has very small errors resulting from misidentification, while the real-time plot of *Calanus* may be in error by ~25 to 35% due to misclassification.

Much of this 'misclassification', however, was due to confusion with 'other copepods', most of which were likely to have been younger stages of *Calanus* not readily identifiable as such in the video images[6]. So the true error was likely to have been much less than 25 to 35%. In addition, this error is due to misclassification of *Calanus* as other taxa, while, as mentioned above, a nearly equal number of individuals from other taxa were misidentified as *Calanus*. These false positives serve to balance the false negatives, so that the reduced abundance of *Calanus* due to false negatives is compensated somewhat by the addition of false positives. While this balance may not be reassuring, it does in fact serve to improve the absolute abundance estimates. The *Calanus* plot (Fig. 4) is, therefore, expected to be a reasonable estimate of the true abundance.

Post-cruise analyses

Assessment of methods for quantifying classifier accuracy

The resubstitution method essentially shows how well the neural network classifier fits the training data and, as such, gives higher overall accuracy than the cross-validation method, which estimates how accurately the classifier is able to sort non-training ROIs (Tables 2 & 3). Post-cruise manual sorting of all the ROIs from VPR-7 (EN302) allowed for a direct comparison of human- and machine-classified images using the hold-out method (Table 4). Initially, it was found that the cross-validation method overestimated the accuracy of the classifier (74%) relative to the true accuracy (63%) obtained using the hold-out method (Table 4). For this classifier, however, training ROIs had been sorted from several tows (Table 4) and only distinctive ROIs for each taxon were selected. Using

[6]Because calanoid copepods share the same general morphology, differentiation of copepod genera/species/life-stages is a more difficult task than differentiating major taxa or particles

Table 4. Confusion matrix for EN302, VPR-7, based on a post-cruise classifier and computed using: (A) cross-validation and (B) hold-out methods. Training ROIs were taken from a mixture of VPR Tows 2, 7, 8, and 9 and 140 total neurons were used. Column and row headings are coded as: 1 = copepod, 2 = rod-shaped diatom chains, 3 = *Chaetoceros* chains, 4 = *Chaetoceros socialis*, 5 = hydroid medusae, 6 = marine snow, 7 = other, TH = Total Human count, TC = Total Computer count, A = Accuracy (% true positive), C/H = Computer/Human total count

	1	2	3	4	5	6	7	TC
(A) Cross-validation								
1	**175**	7	8	5	15	3	28	241
2	6	**226**	0	0	2	0	19	253
3	8	2	**186**	12	22	24	9	263
4	10	1	11	**182**	6	11	20	241
5	21	1	9	0	**173**	22	2	228
6	10	1	18	10	22	**151**	12	224
7	20	10	11	17	8	8	**147**	221
TH	**250**	**248**	**243**	**226**	**248**	**219**	**237**	**1671**
A	70	91	77	81	70	69	62	74
C/H	0.96	1.02	1.08	1.07	0.92	1.02	0.93	1
(B) Hold-out								
1	**2942**	117	4	26	162	52	515	3818
2	346	**3231**	1	20	85	38	372	4093
3	257	11	**345**	153	160	140	315	1381
4	134	23	28	**1557**	74	100	306	2222
5	67	17	25	53	**976**	173	90	1401
6	183	38	38	301	213	**954**	264	1991
7	1503	214	32	270	111	107	**2378**	4615
TH	**5432**	**3651**	**473**	**2380**	**1781**	**1564**	**4240**	**19521**
A	54	88	72	65	54	60	56	63
C/H	0.7	1.12	2.92	0.93	0.79	1.27	1.09	1

the cross-validation method on these distinctive training ROIs, therefore, overestimated the true accuracy of the classifier.

Nonetheless, the true accuracy of the classifier was reasonable for 7 classes. This classifier demonstrates that training ROIs selected in an ad hoc fashion from several different tows (VPR-2, 7, 8, 9) in the same general region can be used to classify a given tow (VPR-7) with reasonable accuracy (Table 4).

The cross-validation estimate of accuracy for the at-sea classifier (84%, Table 2) was significantly higher than the true accuracy in the post-cruise classifier (63%, Table 4). This difference is partially due to the difference in number of taxa classified (5 versus 7), but also was due to the selection of training ROIs at sea, which included a 'blank' category for empty frames due to the VPR breaking the surface on occasion. These blank ROIs were identified with fairly high accuracy (80%) but were over-represented in the at-sea training set so were manually removed from the post-cruise ROI data set. The overall accuracy of the at-sea classifier was likely to have been somewhere between 63 and 84%, but since different taxa were used to build the classifiers, a direct comparison cannot be made.

Direct comparison of cross-validation and hold-out methods for the second post-cruise classifier revealed identical total accuracy (61%, Table 5A,B). The 9 replicate, randomly selected sets of training ROIs (200 per taxon) from VPR-7 yielded means and variances for the cross-validation and hold-out methods (Table 5A,B). Randomness inherent in building the neural network classifier caused some differences in taxon-specific accuracies between the 2 methods, but the overall accuracy of the cross-validation method was found to agree well with the true accuracy from the hold-out method.

To examine the effect of using different training sets, a further test was performed in which a single set of 200 randomly selected training ROIs was used to build 10 replicate classifiers (Table 5C). It can be seen that using the same set of training ROIs did not significantly reduce the variability (cf. Table 5A,B), implying that most of the variance comes from randomizations inherent in building the classifiers.

Selecting training ROIs, such that the number of ROIs per taxon was directly proportional to taxon abundance, did not significantly affect the overall accuracy (Table 5D). Accuracy for the more abundant taxa, such as copepods and *Chaetoceros socialis* colonies, did increase somewhat, but accuracy for rarer taxa, such as *Chaetoceros* chains, was markedly reduced. It was found then that a uniform number of training ROIs is the best overall choice.

Variability inherent in building the classifier comes from 2 sources: (1) randomization of initial position of the neurons and (2) randomization of the order of presentation of the training ROIs to the LVQ algorithm. To determine which source of variation was greater, a further test was performed in which a single set of training ROIs was used to build 2 sets of 10 classifiers. In the first set, classifiers were built using randomized initial positions of neurons and, in the other set, classifiers were built with a single initial distribution of neurons. In both cases, the presentation order of the training ROIs was randomized. For this test, the resubstitution method was used to generate the confusion matrices (Table 6). The variance was found to be the same in the 2 cases, thus it can be inferred that randomization of presentation order of training ROIs is the main source of variability. From these results, it can be concluded that variability in the classification method is due primarily to the nature of the neural network method and not to variability resulting from the random selection of training ROIs.

Table 5. Confusion matrices for EN302, VPR-7. (A–C) Mean confusion matrices. In (A) and (B), the mean matrices shown are computed from 9 individual matrices built with different randomly selected sets of 200 training ROIs and computed using: (A) cross-validation and (B) hold-out method. In (C), the mean matrix is computed from 10 individual matrices each using the same set of 200 randomly selected training ROIs and computed using the hold-out method. (D) confusion matrix computed using the hold-out method and randomly selected training ROIs, where the number of training ROIs for a given taxon is proportional to its average abundance during the tow. $\bar{x}$ and s are mean and standard deviation, $N = 9$ for both (A) and (B), and $N = 10$ for (C). Column and row headings as in Table 4

	1		2		3		4		5		6		7		TC
	$\bar{x}$	s	$\bar{x}$	s	$\bar{x}$	s	$\bar{x}$	s	$\bar{x}$	s	$\bar{x}$	s	$\bar{x}$	s	
(A) Cross-validation															
1	**114**	8	7	1	11	2	2	1	7	2	10	2	50	7	201
2	11	3	**174**	3	2	1	3	2	8	3	3	2	15	4	216
3	4	2	2	1	**121**	4	9	3	22	4	25	4	12	3	195
4	6	2	3	2	12	3	**146**	7	8	3	25	5	19	3	219
5	7	3	4	2	17	4	7	3	**113**	6	27	6	7	3	182
6	10	2	3	1	20	4	18	5	33	4	**97**	9	13	4	194
7	48	4	7	3	17	5	15	4	9	3	13	3	**84**	6	193
TH	**200**		**200**		**200**		**200**		**200**		**200**		**200**		**1400**
A	56		87		60		73		56		48		42		61
C/H	1.01		1.08		0.98		1.1		0.91		0.97		0.97		1
(B) Hold-out															
1	**3604**	397	482	49	26	6	29	18	104	19	95	20	1048	230	5388
2	155	35	**2822**	49	2	1	18	10	59	14	25	3	231	35	3312
3	138	38	20	3	**325**	8	181	38	281	20	184	23	212	36	1341
4	127	32	26	8	26	7	**1757**	82	143	44	181	9	302	58	2562
5	72	14	40	10	13	6	29	7	**829**	52	186	15	97	10	1266
6	116	29	37	13	34	6	119	23	214	35	**758**	35	165	36	1443
7	1771	372	224	33	47	10	247	60	151	19	135	25	**2185**	228	4760
TH	**5983**		**3651**		**473**		**2380**		**1781**		**1564**		**4240**		**20072**
A	60		77		68		73		46		48		51		61
C/H	0.9		0.91		2.84		1.08		0.71		0.92		1.12		1
(C) Single training set															
1	**3763**	142	510	64	31	2	54	11	104	13	115	22	1079	140	5656
2	200	27	**2871**	65	2	2	26	10	67	5	25	6	268	47	3459
3	103	28	17	4	**317**	7	150	29	254	20	172	10	195	5	1208
4	89	23	17	3	23	6	**1703**	53	148	24	186	15	234	23	2400
5	79	18	40	12	17	4	26	5	**825**	26	174	16	93	8	1254
6	84	18	48	4	35	4	142	33	219	23	**760**	23	184	19	1472
7	1665	171	148	12	48	5	279	16	164	18	132	21	**2187**	151	4623
TH	**5983**		**3651**		**473**		**2380**		**1781**		**1564**		**4240**		**20072**
A	62		78		67		71		46		48		51		62
C/H	0.95		0.95		2.55		1.01		0.7		0.94		1.09		1
(D) Training ROIs proportional to abundance															
1	**4190**		691		53		50		178		171		1129		6462
2	121		**2638**		5		30		102		37		207		3140
3	7		3		**161**		18		94		44		23		350
4	107		18		54		**1833**		224		213		274		2723
5	35		25		35		29		**783**		191		70		1168
6	45		11		69		101		175		**640**		101		1142
7	1478		265		96		319		225		268		**2436**		5087
TH	**5983**		**3651**		**473**		**2380**		**1781**		**1564**		**4240**		**20072**
A	70		72		34		77		43		40		57		63
C/H	1.08		0.86		0.74		1.14		0.66		0.73		1.2		1

Accuracy increased only slightly with number of training ROIs used to build the classifier (Table 7). Overall accuracy ranged from 57 to 63% for 50 to 400 training ROIs per taxon, respectively. Thus, development of large training sets, requiring large human sorting effort, does not greatly improve classification accuracy. Lower numbers of training ROIs (<50), however, can greatly reduce classification accuracy.

The number of neurons used to build the classifier, if greater than 6 per taxon, did not appear to substantially affect classification accuracy (Table 8). Accuracy was lower in cases where 3 and 4 neurons per taxon were used. In contrast, use of very large numbers of neurons did not improve classification accuracy.

Likewise, feature length did not affect classification accuracy (Table 9). Feature lengths from 10 to 40 yielded total accuracies of 57 to 60%. It appears, therefore, that the first 10 principal components are sufficient for classification (Table 9).

Much of the classification error results from confusion between the 'Other' category and the rest of the taxa. To examine this effect, a hypothetical case was considered in which the ROIs from the 'Other' category were left completely out of the analysis (Table 10). Without these 'Other' ROIs, overall accuracy increased from 61% (Table 5A) to 75%, showing that the ROIs from the 'Other' category had added significantly to the error in the previous classifier (Table 5A).

Despite the added confusion caused by the 'Other' category, we found that inclusion of an 'Other' category is still necessary. When the 'Other' category is not used (but the 'Other' ROIs are included) and a neuron distance rejection method is used instead, the classification accuracy is much lower. By contrast, when the 'Other' category is included (i.e. training the classifier with samples from the 'Other' category), even when they overlap to a large degree in feature space with the other taxa, the LVQ method does map the neurons for the 'Other' category to these training samples and in doing so reduces the number of false positives.

Accuracy was examined for the 2 dominant taxa, copepods and *Chaetoceros socialis* colonies, using a

Table 6. (A) Mean confusion matrix for EN302, VPR-7. (A) Individual confusion matrices (used to compute this mean matrix) are based on post-cruise classifiers built with the same set of 200 training ROIs but with different initial positions of neurons and computed using the resubstitution method. $\bar{x}$ and s are mean and standard deviation (N = 100). (B) Variability due to the different presentation order of the training ROIs to the LVQ algorithm when building these classifiers. Column and row headings as in Table 4

	1		2		3		4		5		6		7		TC
	$\bar{x}$	s	$\bar{x}$	s	$\bar{x}$	s	$\bar{x}$	s	$\bar{x}$	s	$\bar{x}$	s	$\bar{x}$	s	
A															
1	**152**	5	5	2	4	2	1	1	4	2	3	2	28	4	197
2	5	2	**183**	2	1	1	2	1	4	2	1	1	8	2	204
3	3	1	0	1	**157**	4	6	2	10	3	16	3	9	2	201
4	3	1	2	1	6	2	**173**	3	4	1	14	3	13	3	215
5	6	2	3	1	9	3	2	1	**154**	5	14	3	5	2	193
6	4	2	2	1	14	2	9	2	16	3	**145**	5	8	3	198
7	27	4	5	2	9	3	7	2	8	2	7	2	**129**	5	192
TH	**200**		**200**		**200**		**200**		**200**		**200**		**200**		**1400**
A	76		91		78		86		77		72		64		78
C/H	0.99		1.02		1.01		1.08		0.97		0.99		0.96		1
B															
1	**153**	4	5	1	4	2	1	1	5	2	4	2	28	4	200
2	5	2	**182**	2	0	1	2	1	4	2	1	1	8	2	202
3	2	1	1	1	**157**	5	6	2	11	3	16	3	9	2	202
4	3	1	2	1	6	2	**174**	3	4	2	14	3	13	3	216
5	6	2	3	1	10	3	2	1	**153**	5	15	3	6	2	195
6	4	1	3	1	14	3	9	3	15	3	**143**	5	8	2	196
7	27	4	4	2	9	2	6	2	8	2	7	2	**128**	5	189
TH	**200**		**200**		**200**		**200**		**200**		**200**		**200**		**1400**
A	76		91		78		87		76		71		64		78
C/H	1		1.01		1.01		1.08		0.98		0.98		0.95		1

Table 8. Accuracy as a function of neural number given as percent true positives. (A) EN302, VPR-7. Conditions are the same as for Table 4a, except accuracy is also shown for 42 and 70 neuron cases. Neurons were evenly divided among taxa, i.e. 6, 10 and 20 neurons per taxon for 42, 70 and 140 total neurons. (B) EN323, VPR-3. Neurons were evenly divided among taxa, i.e. 4, 6, 10 and 20 neurons per taxon for 28, 42, 70 and 140 total neurons. (C) EN302, VPR-7. Conditions are the same as for Table 4b. Neurons were evenly divided among taxa, i.e. 3, 4, 6, 10, 15, 20, 30, 50 and 100 neurons per taxon for 21, 28, 42, 70, 105, 140, 210, 350 and 700 total neurons

Neuron #	1	2	3	4	5	6	7	Total
A								
42	67	91	77	77	69	67	60	73
70	69	90	74	81	67	68	64	73
140	70	91	77	81	70	69	62	74
B								
28	65	40	88	93	56	70	46	66
42	67	43	91	94	55	70	53	68
70	68	54	94	90	58	71	50	70
140	66	45	91	90	63	73	52	69
C								
21	45	82	61	55	32	51	60	56
28	48	83	69	65	37	50	62	59
42	46	88	66	59	52	51	56	59
70	53	88	68	58	51	57	52	60
105	47	88	70	55	55	54	58	60
140	47	84	71	60	54	55	56	59
210	48	87	74	52	55	56	57	59
350	50	86	78	56	55	58	56	60
700	46	87	80	56	54	60	56	59

pair-wise analysis (Table 11). When the 2 classes were copepods versus all others, the overall accuracy was 79% and the accuracy for true positives of copepods was 80%. When the 2 classes were *C. socialis* versus all others, the total accuracy was 82%, while the accuracy for true positives of *C. socialis* was 86%.

Abundance versus time plots

Time series plots of taxon abundance for VPR-7 reveal the differences between at-sea and post-cruise classification (Fig. 6A). It is immediately clear that the real-time at-sea classifier yielded abundance patterns (top panel) that are in general very similar to those obtained by manually sorting all the ROIs in the tow (bottom panel). Thus, the general trends in the data can be captured effectively using the real-time imaging methodology, even with an incomplete training set.

The absolute abundances, however, were higher in the real-time case, especially for copepods and

Table 7. Accuracy as a function of number of training ROIs used (per taxon) to build the classifier. EN302, VPR-7. Conditions are the same as for Table 8C for the 70-neuron case. Accuracy is given as percent true positives. Taxa (1 to 7) as in Table 4

Training ROIs used	1	2	3	4	5	6	7	Total
50	63	75	55	62	39	40	44	57
100	60	74	60	66	42	42	47	58
200	60	77	68	73	46	48	51	61
400	63	75	69	75	49	51	56	63

Table 9. Accuracy as a function of the number of features (PCA components) used in the classifier. EN302, VPR-7. Conditions are the same as for Table 8C for the 70 neuron case. Accuracy is given as percent true positives

Feature length	1	2	3	4	5	6	7	Total
10	44	84	69	61	32	42	61	57
15	45	78	69	64	37	45	62	57
20	52	87	68	58	54	50	51	59
25	47	87	67	56	53	54	54	58
30	45	84	73	63	38	51	61	58
35	53	89	69	53	54	54	51	60
40	47	87	69	57	52	57	56	59

Table 10. Confusion matrix for EN302, VPR-7, based on a post-cruise classifier built using 200 randomly selected training ROIs but excluding ROIs from the 'Other' category. This hypothetical case, in which the 'Other' category does not exist in the data set, shows the effect of its removal on classifier accuracy. The confusion matrix was computed using the hold-out method with all ROIs except those from the 'Other' category. Column and row headings as in Table 4

	1	2	3	4	5	6	TC
1	5091	693	37	43	149	105	6118
2	177	2783	5	26	60	25	3076
3	263	21	352	219	256	182	1293
4	107	47	24	1884	137	193	2392
5	85	45	9	31	979	212	1361
6	260	62	46	177	200	847	1592
TH	**5983**	**3651**	**473**	**2380**	**1781**	**1564**	**15832**
A	85	76	74	79	54	54	75
C/H	1.02	0.84	2.73	1.01	0.76	1.02	1

Chaetoceros socialis, owing in part to the lack of categories for 'Marine snow' and 'Other' (Fig. 5A, Table 1), which resulted in these latter taxa being automatically sorted into the other groups. Peaks in *C. socialis* colonies were 25% higher than in the hand-sorted case. Higher copepod and *C. socialis* abundances can be seen clearly by direct comparison of the methods (Fig. 6B).

Initial post-cruise classification reduced the absolute abundance estimates mainly through the addition of 'Marine snow' and 'Other' categories (Table 1) (cf. Fig. 6A, second and bottom panels), which provided the automatic classifier with categories into which the ROIs for these 2 taxa could be sorted. With this classifier (Post-Cruise AutoID 1), however, copepod and *Chaetoceros socialis* abundances were reduced by half and actually underestimated the hand-sorted abundances. This underestimation was due to the fact that the training ROIs for this initial post-cruise classifier were chosen such that only 'good' images of each taxon were selected for training. This biased training process caused the resulting classifier to be selective for 'good' images of each taxon, leading to many false negatives being generated.

Table 11. Pairwise confusion matrix for EN302, VPR-7, based on post-cruise classifier using 200 randomly chosen training ROIs. Each classifier was built with 2 categories: copepods versus all others or *Chaetoceros socialis* versus all others. 200 non-training ROIs then were randomly selected and classified to give the resulting confusion matrix (i.e. hold-out method with 200 ROIs 'held out'). Column and row headings as in Table 4

	Copepods	All others	TC
Copepods	**160**	43	203
All others	40	**157**	197
TH	**200**	**200**	**400**
Accuracy	80	78	79
C/H	1.09	0.92	1
	C. socialis	All others	TC
C. socialis	**173**	44	217
All others	27	**156**	183
TH	**200**	**200**	**400**
Accuracy	86	78	82
C/H	1.02	0.99	1

Random selection of training ROIs from VPR-7 resulted in much closer agreement between automatic and manually derived abundances (Fig. 6A, Post-Cruise AutoID 2). Discrepancies remained, however, and although agreement was very good for higher abundances of *Chaetoceros socialis*, in regions of low abundance, the automatic method overestimated abundance. Likewise, the automated method closely followed trends in rod-shaped diatom abundance but systematically overestimated this abundance and the relative overestimate was greater in the troughs (Fig. 6B).

An attempt was made to correct for classification bias in regions of low relative abundance by applying the method of Solow et al. (2001) (Fig. 6A,B). As discussed in the 'Materials and methods' section, this technique corrects for statistical bias resulting from imperfect classification that causes taxa in low relative abundance to be overestimated. Application of this method met with limited success. Abundances of copepods and hydroids were not improved, while those of rod-shaped diatoms were improved in the troughs but overestimated in the peaks. *Chaetoceros socialis* was underestimated in the low-abundance regions. In general, this correction method had no obvious improvement on these abundance estimates.

Although the abundance estimates based on computer classification deviated from the hand-sorted results, the changes in natural abundance were generally much larger, so that the trends in the abundance data were quantified reasonably well, especially for the more variable diatom taxa (Fig. 6B). For all taxa, the relative error in abundance decreased in areas of high abundance (compare red and blue curves in Fig. 6B). This effect is examined directly in Fig. 6C, where, for each taxon, the relative error is plotted versus relative abundance (top panel). Each individual data point in this figure corresponds to an individual towyo (double-oblique vertical cast) (Fig. 3). Thus, the data are comparable to a series of 254 double-oblique plankton tows ('tow' durations are about 6 min each). The average abundance value for each 'tow' was determined for computer- and human-classified results. This plot shows clearly that the relative error falls off markedly with increasing relative abundance. When the relative abundance of a taxon is above 20 to 25%,

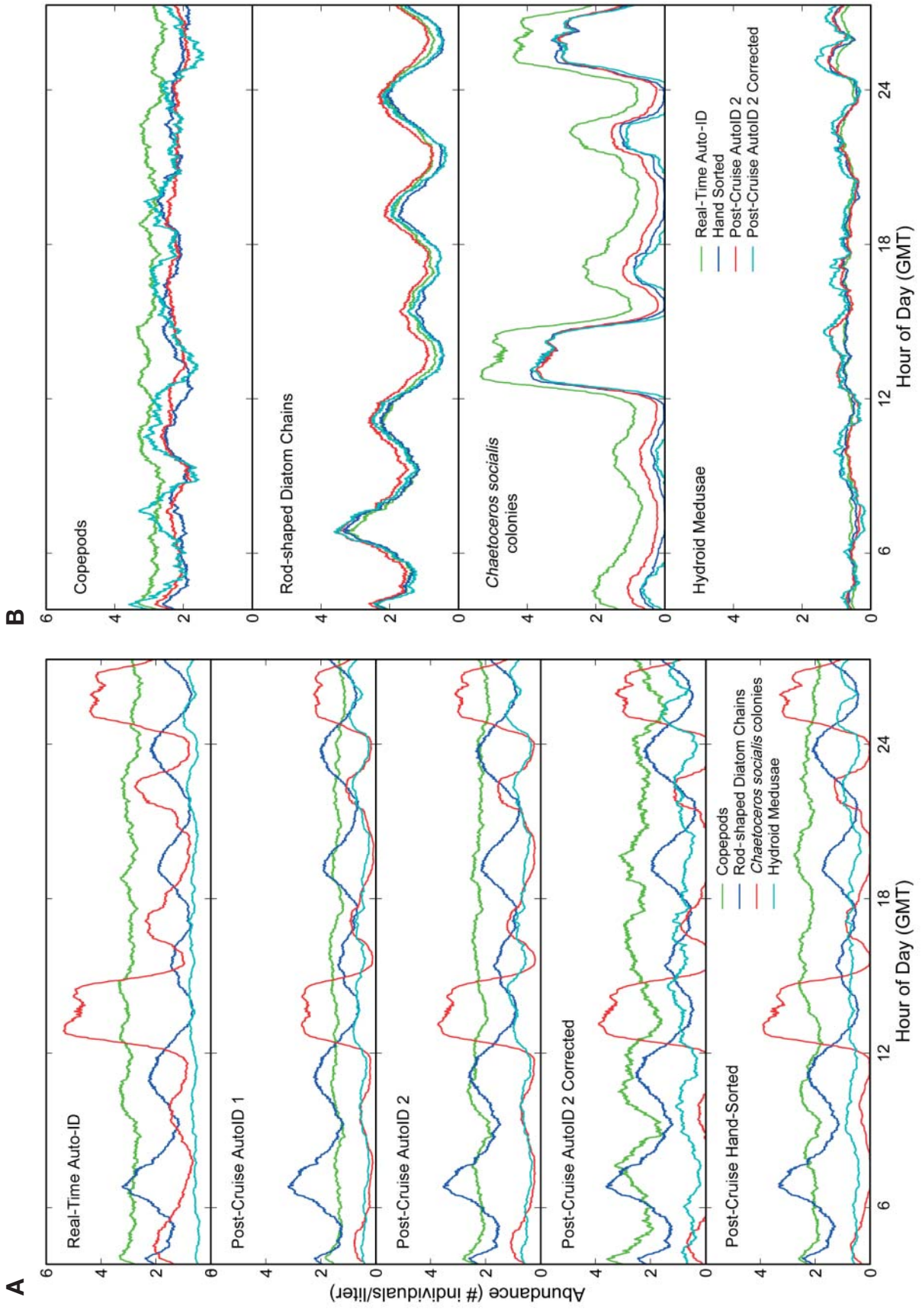
A
Real-Time Auto-ID
Post-Cruise AutoID 1
Post-Cruise AutoID 2
Post-Cruise AutoID 2 Corrected
Post-Cruise Hand-Sorted
Abundance (# individuals/liter)
Copepods
Rod-shaped Diatom Chains
Chaetoceros socialis colonies
Hydroid Medusae
Hour of Day (GMT)
B
Copepods
Rod-shaped Diatom Chains
Chaetoceros socialis colonies
Hydroid Medusae
Real-Time Auto-ID
Hand Sorted
Post-Cruise AutoID 2
Post-Cruise AutoID 2 Corrected
Hour of Day (GMT)

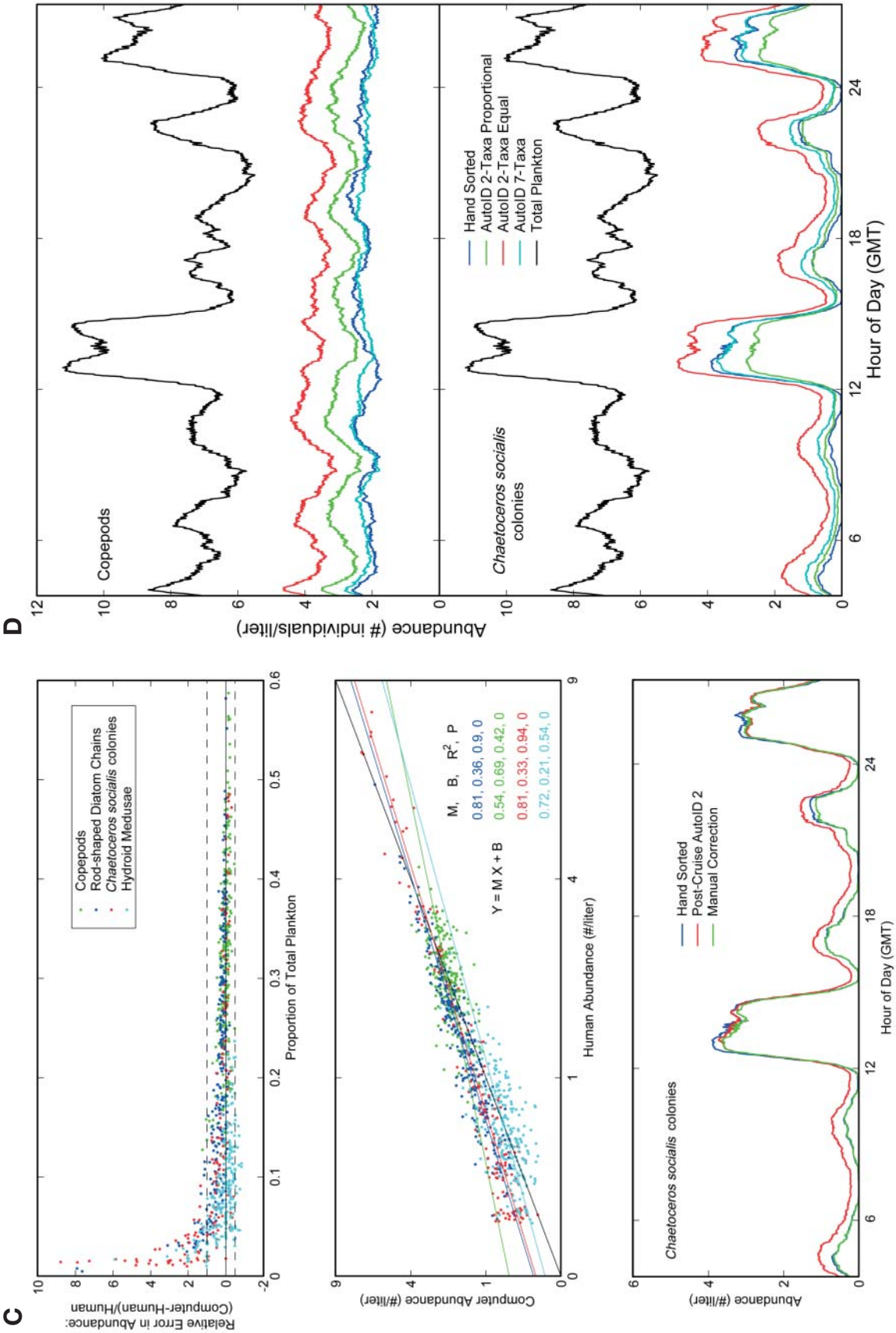

Fig. 6. Time-series abundance plots from the Great South Channel study (VPR-7). (A) Abundance of 4 dominant taxa as determined by: top panel: real-time at-sea classifier; second panel: first post-cruise classifier (Tables 1 & 4); third panel: second post-cruise classifier (Tables 1 & 5); fourth panel: second post-cruise classifier plus application of the Solow et al. (2001) correction method; bottom panel: human-classified result. (B) Same results as in (A) but with individual taxa plotted together. (C) Deviations in abundance from the human classified result shown in (A). (D) Abundances derived from pair-wise (2-class) classifiers for: top panel: copepods versus all other taxa; bottom panel: *Chaetoceros socialis* versus all other taxa. Also plotted in both panels are the 7-taxa and human-classified results

the relative error due to misclassification falls well within the natural variation for replicate plankton tows, which typically vary by at least a factor of 0.5 to 2 (relative error = 0.5 to 1; see dashed lines in Fig. 6C) (e.g. Wiebe & Holland 1968). Regression analysis directly comparing computer and human abundance estimates reveals that, for all taxa, variation due to misclassification is significantly smaller than that due to natural changes in abundance (Fig. 6C, middle panel). For the 2 diatom taxa, variability due to misclassification was ≤10% of the total variance, and even for the less variable copepods and hydroid medusa, about half of the variation was due to changes in natural abundance, implying that significant trends in natural abundance are quantifiable despite the higher misclassification error.

We also have used a manual correction step to quickly remove errors due to computer misclassification of a given taxon. This method involves using a point and click user interface to manually remove false positives from the automatic identification results for that taxon. Abundances are then computed from the corrected identification results and these abundances are divided by the probability of detection (% true positive) for that taxon obtained from the confusion matrix. The effort involved in removal of false positives is minimal. We found from timed trials that a trained observer can visually scan through 100 to 200 ROIs per minute, removing false positives. In regions of high relative abundance, the proportion of false positives is low, facilitating their removal, but these areas also have more ROIs. By contrast, areas of low abundance have a high proportion of false positives, but the number of ROIs is lower. As an example, in VPR-7, the number of ROIs automatically classified as copepods ranged from 10 to 387 h^{-1}, requiring 0.1 to 2 min h^{-1} to remove the false positives. Thus, this manual step can be done quickly, allowing for real-time on-the-fly correction. This method eliminates most of the error due to computer misclassification and greatly improves the accuracy for the abundance of the corrected taxon (e.g. *Chaetoceros socialis*, Fig. 6C, bottom panel).

Although the pair-wise classifiers for copepods and *Chaetoceros socialis* had apparently higher accuracy based on their confusion matrices (Table 11), this was due largely to the reduction in number of categories from 7 to 2 and did not increase the accuracy in terms of abundance (Fig. 6D). In fact, this approach made the agreement between automatic and manual methods much worse, with the automatic sorting resulting in systematic overestimation of copepods. *C. socialis* abundance peaks were underestimated while its troughs were overestimated. Two 2-taxa classifiers were used, one built with 200 training ROIs for each taxon and the other with the number of training ROIs proportional to taxon abundance. Neither of these 2-taxa classifiers worked very well. The 7-taxa classifier clearly outperformed them (Fig. 6D).

Summary of classification analysis

The analysis of different approaches and criteria permits the formulation of some general guidelines for establishing training sets and classifiers for data sets similar to ours: (1) Classifier accuracy depends on a variety of factors. The range in overall accuracy was 60 to 70% for 7 taxa and 79 to 82% for 2 taxa, with accuracies for individual taxa ranging between 45 and 91%. (2) The minimum number of ROIs needed for training is far less than might be considered intuitively, with a training set of 200 images per category (7% of total ROIs) performing as well as larger sets (but note that performance fell off below 50 images per category). (3) Equal numbers of training ROIs per category produces more accurate classifiers than using category abundances that were proportional to observed abundances. (4) Increasing the number of neurons per category in the classifier beyond 6 or the feature length beyond 10 does not improve classification accuracy. (5) Using an ad hoc versus random selection of training ROIs does not significantly affect true accuracy (cf. Tables 4B & 5B), but it is important to select representative ROIs, rather than only distinctive ones. (6) Classifier variability is affected mainly by presentation order of the training ROIs and not by initial neuron positions. (7) Including an 'Other' category increases accuracy. Abundance estimates are more accurate when using all categories of taxa and particles present (grouping rare categories into 'Other'), although overall classification accuracy naturally decreases as the number of categories is increased. (8) Errors due to misclassification by computer are typically lower than the natural variations in dominant plankton. (9) A rapid manual correction step can be used to correct errors in abundance due to computer misclassification. (10) In general, artificial neural networks are able to learn from labeled samples and can provide reliable abundance estimation for dominant taxa.

Significance and future directions

The field data presented here reveal high-resolution spatio-temporal patterns in plankton and illustrate the utility of rapid automated approaches to measuring abundance of planktonic taxa in a dynamical environment. The machine identification accuracy was found to be sufficient for quantitative measurement of abundance patterns for dominant plankton taxa. The ability

to observe plankton distributions in real time allows plankton ecologists to interactively alter the sampling design as new information is acquired. This capability is particularly important in mapping plankton patches and sampling plankton distributions and behaviors in these characteristically ephemeral environments. Optical sampling technology enables plankton ecologists to sample plankton distributions quickly over the same broad range of time and space scales as their associated environmental variables, thus improving our understanding of factors controlling aquatic ecosystem dynamics. Care must be taken when applying this approach for non-dominant taxa, since the rate of false positives will be relatively large, even when the statistical correction method is applied. In this case, a rapid manual correction step can be used. For dominant taxa, machine classification was found to be a viable approach, with accuracies similar to those reported for humans (43 to 95%, Culverhouse et al. 2003). We are actively researching ways to improve the image quality and identification accuracy, including incorporation of other features and classification methods.

Acknowledgements. We greatly appreciate the support of the officers and crew of the RV 'Endeavor'. P. Alatalo and A. Girard provided valuable assistance both at sea and in the laboratory. This work was funded by Office of Naval Research grants N00014-93-10602 and N00014-98-10032 and National Science Foundation grants OCE-9632596, OCE-9806498, OCE-9820099 and OCE-0000580.

LITERATURE CITED

Ashjian CA, Davis CS, Gallager SM, Alatalo P (2001) Distribution of plankton, particles, and hydrographic features across Georges Bank described using the Video Plankton Recorder. Deep-Sea Res II 48:245–282

Beardsley R, Davis CS, Irish JD, Lough RG, Mountain D, Wiebe PH (1992) US GLOBEC Implementation Plan for the Northwest Atlantic Field Program

Benfield MC, Davis CS, Wiebe PH, Gallager SM, Lough RG, Copley NJ (1996) Comparative distributions of calanoid copepods, pteropods, and larvaceans estimated from concurrent Video Plankton Recorder and MOCNESS tows in the stratified region of Georges Bank. Deep-Sea Res II 43:1925–1946

Cover TM (1969) Learning in pattern recognition. In: Watanabe S (ed) Methodologies of patterns recognition. Academic Press, New York, p 111–132

Culverhouse PF, Williams R, Reguera B, Herry V, Gonzalez-Gill S (2003) Do experts make mistakes? A comparison of human and machine identification of dinoflagellates. Mar Ecol Prog Ser 247:17–25

Davis CS (1984) Predatory control of copepod seasonal cycles on Georges Bank. Mar Biol 82:31–40

Davis CS (1987) Components of the zooplankton production cycle in the temperate ocean. J Mar Res 45:947–983

Davis CS, Gallager SM, Berman MS, Haury LR, Strickler JR (1992a) The Video Plankton Recorder (VPR): design and initial results. Arch Hydrobio Beih 36:67–81

Davis CS, Gallager SM, Solow AR (1992b) Microaggregations of oceanic plankton observed by towed video microscopy. Science 257:230–232

Davis CS, Gallager SM, Marra M, Stewart WK (1996) Rapid visualization of plankton abundance and taxonomic composition using the Video Plankton Recorder. Deep-Sea Res II 43:1947–1970

Denman KL, Herman AW (1978) Space–time structure of a continental shelf ecosystem measured by a towed porpoising vehicle. J Mar Res 36:693–714

Dennett MR, Caron DA, Michaels AE, Church M, Gallager SM, Davis CS (2002) Video Plankton Recorder reveals high abundance of colonial radiolaria in surface waters of the central north Pacific. J Plankton Res 24:797–805

Fasham MJR (1978) The statistical and mathematical analysis of plankton patchiness. Oceanogr Mar Biol Annu Rev 16: 43–79

Fukunaga K, Hummels DM (1989) Leave-one-out procedures for nonparametric error estimates. IEEE Trans Pattern Anal Machine Intelligence 11:421–423

Gallager SM, Davis CS (2003) Innovative instrumentation in biological oceanography: the role of zooplankton in global ecosystem dynamics: comparative studies from the world's oceans. ICES, PICES, GLOBEC, Gijon

Gallager SM, Davis CS, Epstein AW, Solow A, Beardsley RC (1996) High-resolution observations of plankton spatial distributions correlated with hydrography in the Great South Channel, Georges Bank. Deep-Sea Res II 43: 1627–1664

Gallager SM, Yamazaki H, Davis CS (2004) Contribution of fine-scale vertical structure and swimming behavior to formation of plankton layers on Georges Bank. Mar Ecol Prog Ser 267:27–43

GLOBEC (1991) Initial science plan. University of California, Berkeley

Gonzalez RC, Wintz P (1987) Digital image processing. Addison Wesley, New York

Hardy A (1956) The open sea. Collins, London

Haury LR, McGowan JA, Wiebe PH (1978) Patterns and processes in the time–space scales of plankton distributions, in spatial patterns in plankton communities. In: Steele JH (ed) Spatial patterns in plankton communities. Plenum Press, New York, p 277–327

Herman AW (1992) Design and calibration of a new optical plankton counter capable of sizing small zooplankton. Deep-Sea Res 39:395–415

Holliday DV, Pieper RE, Kleppel GS (1989) Determination of zooplankton size and distribution with multifrequency acoustic technology. J Cons Int Explor Mer 41:226–238

Hu MK (1962) Visual pattern recognition by moment invariants. IRE Trans Inform Theory 8:179–187

Huntley ME, Zhou M, Nordhausen W (1995) Mesoscale distribution of zooplankton in the California Current in late spring, observed by optical plankton counter. J Mar Res 53:647–674

Jain AK, Puin RPW, Mao J (2000) Statistical pattern recognition: a Review. IEEE Trans Pattern Anal Machine Intelligence 22:4–37

Kohonen T, Barna G, Chrisley R (1988) Statistical pattern recognition with neural networks: benchmarking studies. In: Proc Conf Neural Networks (ICNN), 1:61–68, Los Alamitos, CA. IEEE Computer Society Press

Ledwell J (1999) US GLOBEC: Cruise Report for R/V Endeavor Cruises En323 and EN324, US GLOBEC Georges Bank Program Office. WHOI, Woods Hole, MA

Lynch DR, Naimie CE, Ip JT, Lewis CV and 16 others (2001) Real-time data assimilative modeling on Georges Bank. Oceanography 14:65–77

Mackas DL, Denman KL, Abbott MR (1985) Plankton patchiness: biology in the physical vernacular. Bull Mar Sci 37: 652–674

Marine Zooplankton Colloquium (1989) Future directions in marine zooplankton research: a perspective. Mar Ecol Prog Ser 55:197–207

McGillicuddy DJ, Kosnyrev VK (1999) US GLOBEC: Georges Bank real-time modeling on cruises EN323 and EN324, May–June 1999. WHOI, Woods Hole, MA

Norrbin MF, Davis CS, Gallager SM (1996) Differences in fine-scale structure and composition of zooplankton between mixed and stratified regions of Georges Bank. Deep-Sea Res II 43:1905–1924

Ohman MD, Smith PE (1995) A comparison of zooplankton sampling methods in the CalCOFI time series. Reports of California Cooperative Oceanic Fisheries Investigations (CALC CALCOFI REP) 36:153–158

Omori M, Ikeda T (1984) Methods in marine zooplankton ecology. Wiley, New York

Pingle KK (1969) Visual perception by a computer. In: Grasselli A (ed) Automatic interpretation and classification of images. Academic Press, New York, p 277–284

Platt T, Denman KL (1978) The structure of pelagic marine ecosystems. Rapp P-V Reun Cons Int Explor Mer 173:60–65

Pratt WK (1976) Digital image processing. Wiley, New York

Rothschild BJ (ed) (1988) Toward a theory on biological-physical interactions in the world ocean. Kluwer, Boston

Schulze P, Strickler JR, Bergstrom BI, Berman M and 11 others (1992) Video systems for in situ studies of zooplankton. Arch Hydrobiol Beih 36:1–21

Sherman K (1980) MARMAP, a fisheries ecosystem study of the Northwest Atlantic fluctuations in ichthyoplankton-zooplankton components and their potential for impact on the system. In: Diemer FP, Vernberg FJ, Mirkes DZ (eds) Advanced concepts in ocean measurements of marine biology. University of South Carolina Press, Columbia, p 3–37

Sieracki M, Gifford D, Gallager SM, Davis CS (1998) Observations on a dense patch of the diatom, *Chaetoceros socialis*, on the southern flank of Georges Bank: distribution, colony structure and grazing losses. Oceanography 11:30–35

Silvert W, Platt T (1980) Dynamic energy flow model of the particle size distribution in pelagic ecosystems. In: Kerfoot WC (ed) Evolution and ecology of zooplankton communities. University Press of New England, Hanover, NH, p 754–763

Solow A, Davis CS, Hu Q (2001) Estimating the composition of a sample when individuals are classified with error. Mar Ecol Prog Ser 216:309–311

Sprules WG, Munawar M (1986) Plankton size spectra in relation to ecosystem productivity, size, and perturbation. Can J Fish Aquat Sci 43:1789–1794

Tang X, Stewart WK, Vincent L, Huang H, Marra M, Gallager SM, Davis CS (1998) Automatic plankton image recognition. Artificial Intelligence Rev 12:177–199

Villareal TA, Pilskaln C, Brzezinski M, Lipschultz F, Dennett M, Gardner GB (1999) Upward transport of oceanic nitrate by migrating diatom mats. Nature 397:423–425

Vincent L (1993) Morphological grayscale reconstruction in image analysis: application and efficent algorithm. IEEE Trans Image Processing 2:176–201

Warner A, Hays G (1994) Sampling by the Continuous Plankton Recorder survey. Prog Oceanogr 34:237–256

Wiebe PH, Holland WR (1968) Plankton patchiness: effect of repeated net tows. Limnol Oceanogr 13:315–321

Wiebe PH, Mountain DG, Stanton TK, Greene CH, Lough G, Kaartvedt S, Dawson J, Copley N (1996) Acoustical study of the spatial distribution of plankton on Georges Bank and the relationship between volume backscattering strength and the taxonomic composition of the plankton. Deep-Sea Res II 43:1971–2001

Zahn CT, Roskies RC (1972) Fourier descriptor for plane closed curves. IEEE Trans Computers 21:269–281

Editorial responsibility: Kenneth Sherman (Contributing Editor), Narragansett, Rhode Island, USA

Submitted: December 29, 2003; Accepted: June 7, 2004
Proofs received from author(s): December 14, 2004